Hydrogen Bonding Stabilized Self-Assembly of Inorganic Nanoparticles: Mechanism and Collective Properties

Mingli Yue,[†] Yanchun Li,[‡] Ying Hou,[†] Wenxin Cao,[§] Jiaqi Zhu,[§] Jiecai Han,[*,§] Zhongyuan Lu,[*,‡] and Ming Yang[*,†]

[†]Key Laboratory of Microsystems and Micronanostructures Manufacturing, Harbin Institute of Technology, 2 Yikuang Street, Harbin 150080, PR China, [‡]State Key Laboratory of Supramolecular Structure and Materials, Institute of Theoretical Chemistry, Jilin University, Changchun 130023, PR China, and [§]Center for Composite Materials and Structures, Harbin Institute of Technology, 2 Yikuang Street, Harbin 150080, PR China

ABSTRACT Developing a simple and efficient method to organize nanoscale building blocks into ordered superstructures, understanding the mechanism for self-assembly and revealing the essential collective properties are crucial steps toward the practical use of nanostructures in nanotechnology-based applications. In this study, we showed that the high-yield formation of ZnO nanoparticle chains with micrometer length can be readily achieved by the variation of solvents from methanol to water. Spectroscopic studies confirmed the solvent effect on the surface properties of ZnO nanoparticles, which were found to be critical for the formation of anisotropic assemblies. Quantum mechanical calculations and all atom molecular dynamic simulations indicated the contribution of hydrogen bonding for stabilizing the structure in water. Dissipative particle dynamics further revealed the importance of solvent—nanoparticle interactions for promoting one-dimensional self-assembly. The branching of chains was found upon aging, resulting in the size increase of the ensembles and network formation. Steady-state and time-resolved luminescent spectroscopes, which probed the variation of defect-related emission, revealed stronger Forster resonance energy transfer (FRET) between nanoparticles when the chain networks were formed. The high efficiency of FRET quenching can be ascribed to the presence of multiple energy transfer channels, as well as the short internanoparticle distances and the dipole alignment.

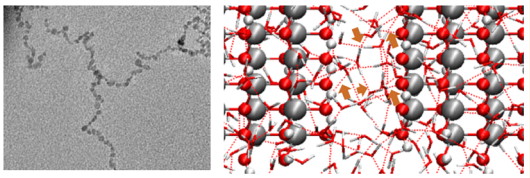

KEYWORDS: self-assembly · ZnO · nanoparticles · anisotropic structure · one-dimensional · chains · hydrogen bonding · molecular dynamics

Inorganic nanoparticles (NPs) represent one of the most versatile building blocks for the construction of functional nanoscale devices due to their controllable sizes/shapes,[1] modifiable surface chemistry[2] and intriguing optical,[3] electrical,[4] magnetic,[5] catalytic[6] and mechanical properties.[7] Self-assembly of NPs, which to some extent, mimics their biological counterpart such as proteins,[8] remains the most facile and flexible way to realize the well-organized patterns of nanostructures. The ability of NPs to self-assemble under suitable environment has resulted in a broad spectrum of nanostructures including chains,[9] sheets,[10] and artificial solids,[11] just to name a few. Successful manipulation of such spontaneous process allows the emergence of novel functionalities thanks to the synergetic effect, which however typically requires the intricate control over the interplay between NPs due to the versatility of interparticle interactions and also their interdependent nature.[12] A better understanding of the principles for self-assembly at the molecular level will be therefore much needed for the more effective utilization of multiple nanoscale forces.

One-dimensional (1D) assemblies, as against two-dimensional (2D) and three-dimensional (3D) assemblies with typical close-packed patterns,[13−15] represent a prototype for the study of unique transfer properties, critical for the performance of electronic/optical nanodevices.[16] Recent years have also seen much increasing attention for probing plasmonic coupling in metallic NP chains due to the "hot-spot" effect.[17−21] The construction of 1D assembly may require linear template,[22−24] whereas magnetic NPs can be aligned under external field thanks to the presence of magnetic dipole moment.[25−28] Spontaneous formation of such directional structures has also been

* Address correspondence to hanjc@hit.edu.cn, luzhy@jlu.edu.cn, yangm@hit.edu.cn.

Received for review January 16, 2015 and accepted May 19, 2015.

Published online May 19, 2015
10.1021/acsnano.5b00344

observed by using surface modified NPs triggered by polymerization,[29−31] specific recognition[32−34] or phase segregation.[18,35,36] The recent demonstrated linear structures of octapods[37] and helical ribbons of rod-like fd viruses[38] highlight the importance of intrinsic characteristics of nanocolloids such as shapes[39] and chirality in guiding 1D organization.

Electric dipole moment arising from the asymmetric crystal structure is another essential factor in inducing the formation of various 1D nanostructures such as chains both experimentally[9,40] and theoretically.[41,42] Chain-like structures can be regarded as the result of head-to-tail dipolar arrangement to minimize the overall potential energy[43] and could be an intermediate state for the transition from NPs to nanorods.[40] However, even for NPs which possess relatively large electric dipole moment, the formation of chain-like structure is not usually observed. Possible reasons for this could include the following: (1) The thick organic shells used to control the growth of NPs during the synthesis can deplete the interparticle dipolar interactions. For example, the synthesis of ZnO nanopyramids typically employed the organic molecules as stabilizers.[44,45] In these systems, chain-like structures of nanopyramids were never observed. In contrast, we recently synthesized ZnO nanopyramids in methanol without using any stabilizers and observed the interesting assembly and disassembly processes.[43] (2) The presence of other repulsive forces such as electrostatic interactions can smear the attractive dipole−dipole interactions. A typical case is the self-organization of CdTe nanoparticles into pearl-like nanostructures, which can only be observed after nonsolvent washing.[9] The weakening of the electrostatic repulsion between NPs by partial removal of negative charged surface stabilizers was believed to facilitate the chain formation. (3) Other long-range isotropic attractions such as van der Waals forces may disturb the short-range dipolar interaction, and only precipitates with less defined structure can be obtained.

To favor 1D self-assembly of NPs possessing electric dipole moment, one possible way is to increase the magnitude of dipolar interactions by using larger NPs. However, this would also result in the increase of van der Waals forces, leading to less structural control. Alternatively, additional attractive attributes may be deliberately added to stabilize the structure. Among the noncovalent interactions, the strongest is hydrogen bonding. Interestingly, in the regime of biomolecules, hydrogen bonding has been suggested to be crucial for the formation of various superstructures such as nanotubes and nanofibers,[46] typically coupled with other intermolecular interactions, for instance, pi-pi stacking[47] and hydrophobic interactions.[48,49] We speculate that for the colloids of inorganic NPs, the cooperation of hydrogen bonding with dipolar interactions may also be an effective way to achieve 1D superstructure.

Besides the fundamental interest in understanding the mechanism of self-assembly and design principles of ordered structures, it would be also essential to reveal interesting collective properties of organized NP assemblies.[50,51] Superstructures of semiconductor NPs with unique quantum mechanical properties have received tremendous attention due to the interparticle coupling, which allows their effective communications.[52,53] Studies in this field were focused on the colloidal NPs including CdSe,[52,53] CdSe/ZnS,[54] CdTe,[55] and InP[56] with typical narrow band gap emission. Extended arrays of colloidal quantum dots such as artificial solids from CdSe NPs and gradient NPs with different sizes are typical examples of how energy transfer between quantum dots can be strengthened and controlled by the manipulation of nanoscale arrangement.[52,53] However, as far as we know, there is no previous report on the study of coupling effect in the organized structures from colloidal NPs with wide band gap typically larger than 3 eV.

In this contribution, we showed that the interparticle hydrogen bonding in water can promote the spontaneous formation of long ZnO NP chains. Molecular dynamic (MD) simulation confirmed the role of hydrogen bonding in stabilizing the chain-like structure and dissipative particle dynamics (DPD) simulation further revealed the importance of NP-solvent interactions in guiding anisotropic self-assembly. The first example of energy transfer in ZnO NP assemblies was also demonstrated by probing the variation of visible emission. Both steady and transient optical spectra indicated stronger coupling of NPs in highly branched ZnO NP chains with multiple energy transfer channels.

RESULTS AND DISCUSSION

ZnO as an important wide band gap semiconductor has attracted so much interest during the past years. Its great potentials for a variety of practical applications, such as in catalysis,[57] solar energy conversion,[58] sensors,[59] optoelectronic[60] and piezotronic devices[61] have been demonstrated. Low-dimensional ZnO nanostructures were extensively investigated due to their distinct anisotropic physical properties.[62−64] The electric dipole moment of ZnO has been generally correlated with their habitual 1D crystal growth. A previous study showed that oriented attachment of ZnO NPs occurred before the transition from NPs to nanorods only in a concentrated solution after reflux.[40] According to the authors, linear assemblies in all aggregated particles were not observed. Furthermore, the length of ZnO NP chains was observed to be very short and only consisted of several NPs.[40] However, other NPs such as gold[65,66] and cubic CdTe NPs,[9] which possess relatively small dipole moment induced either by surface chemistry[67] or truncations,[68] have been shown to spontaneously form long chains of NPs. Interestingly, we found that virtually all ZnO NPs spontaneously

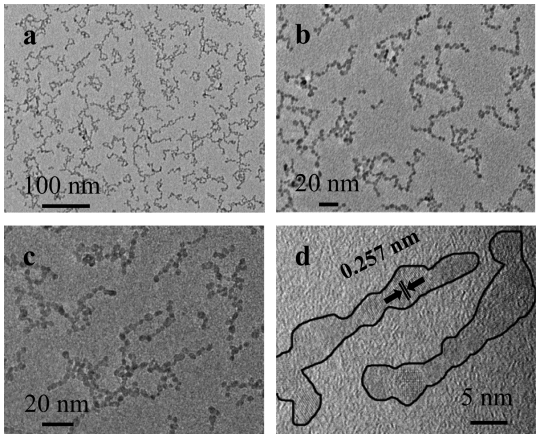

Figure 1. TEM images of ZnO NPs in water.

self-assembled into chain-like structures in water (Figure 1). The length of these chains is in the order of several hundred nanometers (Figure 1). ZnO NPs in these chains preferred to align along *c*-axis as evidenced by the lattice spacing of *ca*. 0.257 nm, which corresponds to the distance between two (0002) crystal planes (Figure 1d). Such observation indicated that the presence of electric dipole moment is critical for the anisotropic organization in water. Analogous with the previous study,[40] no formation of distinct assemblies can be observed in the as-prepared alcoholic colloidal dispersion consisted of 3−5 nm ZnO NPs (Figure S1, Supporting Information).

As the spontaneous formation of chain-like structures was induced by changing the solvent, we first tried to understand the environmental influence on the interparticle interactions including electrostatic, dipolar, charge-dipole and van der Waals forces, which are typically involved in the Derjaguin−Landau−Verwey−Overbeek (DLVO) theory for the estimation of stability of colloidal solution. Assuming that ZnO NPs are monodisperse spherical NPs, we have the following expressions to describe the potential energies of different interactions: the electrostatic repulsion potential (V_{elec}), the dipolar interaction potential (V_{dipole}), the charge−dipole interaction potential ($V_{charge-dipole}$) and the van der Waals attraction potential (V_{vdW}).

$$V_{elec}(r) = 2\pi\varepsilon_s\varepsilon_o a\Psi_o^2 \ln\{1+\exp[-a\kappa(R-2)]\} \quad (1)$$

$$V_{dipole}(r) = -\frac{\mu^2}{2\pi\varepsilon_s\varepsilon_o R(R^2-4a^2)} \quad (2)$$

$$V_{charge-dipole}(r) = -\frac{Q^2\mu^2}{6(2\pi\varepsilon_s\varepsilon_o)^2 k_B T r^4} \quad (3)$$

$$V_{vdW}(r) = -\frac{A_H}{6}\left[\frac{2}{R^2-4}+\frac{2}{R^2}+\ln\frac{R^2-4}{R^2}\right] \quad (4)$$

Herein, ε_s is the relative dielectric constant of the solvent, ε_o is the dielectric constant of vacuum, a is the radius of NPs, Ψ_o is the surface potential of the particle, κ is the inverse Debye length, r is the center-to-center separation of neighboring NPs of radius a, $R = r/a$, μ is the dipole moment, Q is the effective surface charge of the NPs, k_B is the Boltzmann constant, T is the absolute temperature, A_H is the Hamaker constant.

According to the eqs 1, 2, 3, the replacement of methanol ($\varepsilon_s = 32.6$) with water ($\varepsilon_s = 80.4$) will result in the increase of electrostatic interactions and the decrease of dipolar and charge-dipole interactions. van der Waals forces have no correlation with solvent conditions (eq 4). The quantitative analysis based on DLVO theory indicated an overall shift of interparticle forces toward repulsion when methanol was substituted by water. We therefore foresee that besides the interparticle interactions we considered so far, there must be other attractive forces contributing to the chain formation in water.

The above discussions led us to turn our attention to the investigation of solvent effect on the properties of ZnO NPs, which may favor an overall shift of interparticle forces toward attraction. Previous studies have shown that solvents not only affect the solution parameters but also influence the physical and chemical properties of NP surfaces. The notable example of solvent effect on the stability of NPs is the nonsolvent induced assembly or precipitation, during which the relative strength of particle−particle and particle−solvent interactions are adjusted along with the conformation change of organic stabilizers.[30,69−71] For oxide NPs, the use of water as solvent is believed to induce water adsorption due to the acid−base properties of the oxides.[72] We first carried out IR spectra measurement to study the surface species of ZnO NPs obtained from different solvents. It was found that the pronounced variation of IR spectra is the much enhanced intensity of the broad feature around 3400 cm^{-1} (Figure S2), indicating the increase of the density of the hydroxyl when the solvent was changed from methanol to water. The diminishing of broad peaks from 2500 to 3000 cm^{-1} for ZnO NPs in water compared with that in methanol was also observed (Figure S2). As the bands due to asymmetric and symmetric CH stretching vibrations exist in this range, such spectral change implied the replacement of chemisorbed methanol by water absorption, which has been also suggested in previous studies.[73,74] The comparison of O_{1s} XPS spectra of ZnO NPs from different solvents further confirmed the increase of surface hydroxyl groups in water (Figure S3). The presence of five different O_{1s} peaks after deconvolution was observed for ZnO NPs obtained from methanol (Figure S3a), in good agreement with other report.[75] The peak around 529.5 eV can be attributed to the H bonds at certain crystal planes.[76] The peak located at 530.9 eV is attributed to the O^{2-} ions surrounded by Zn atoms. The peaks at 531.5 and

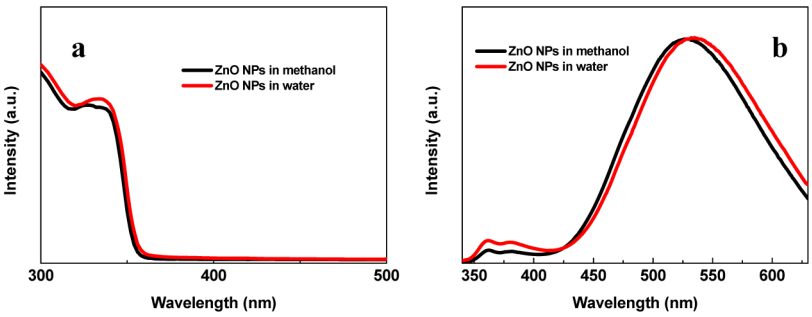

Figure 2. (a) UV−vis and (b) photoluminescence spectra of ZnO NPs in methanol and water, respectively.

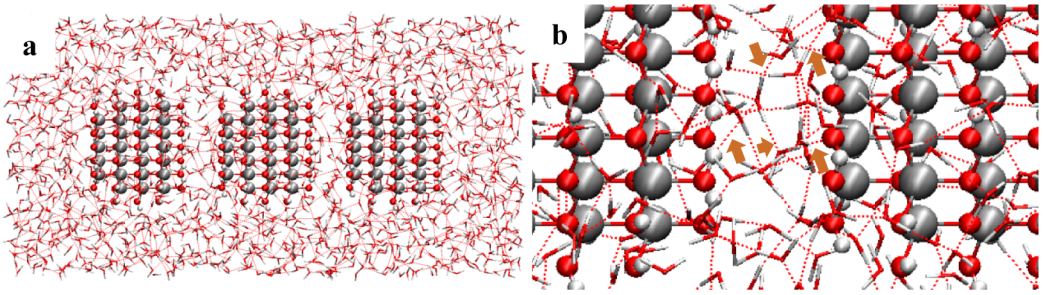

Figure 3. MD simulation snapshots of ZnO NPs in water. Gray atom: Zn, red atom: O, white atom: H, red dashed lines: hydrogen bonds. The arrows in (b) indicate the connection of two NPs by water through the network of hydrogen bonding.

532.2 eV can be associated with the presence of −OH groups on the surface of ZnO NPs. The small peak around 533.7 eV can be ascribed to other surface absorbed species such as COO^-. Compared with O_{1s} XPS in methanol, the areas of the peaks at 531.5 and 532.5 eV are much increased, which can be explained by the presence of vast amount of hydroxyl groups on the surface of NPs in water (Figure S3b).

We further performed absorption and emission spectra of ZnO NP dispersions. UV−vis spectra of ZnO NPs showed a shift of the first exciton transition peak from *ca.* 336 nm to *ca.* 334 nm when the solvent was changed from methanol to water (Figure 2a). As there is no obvious size change according to TEM observations (Figure 1 and S1), such shift can be related to the variation of environmental dielectric constant.[77] The photoluminescence spectra of ZnO NPs in methanol and water both showed a dominant emission in the visible range (Figure 2b), which originated from surface defects.[78] A minimal excitonic emission around 360 nm was also observed whose position remained unchanged (Figure 2b). A bathochromic shift from *ca.* 526 nm to *ca.* 535 nm was detected for visible emission accompanying the solvent change from methanol to water. As the surface species have dramatic influence on the emission spectra of NPs due to the existence of different surface states, such shift further confirmed the variation of surface properties. Previous study has shown that green emission (*ca.* 593 nm) can be directly correlated with surface hydroxyl groups.[75] It is therefore believed that the shift toward long-wavelength emission can be a result of hydrolysis process in water.

The presence of surface hydroxyl groups may favor the formation of hydrogen bonds between ZnO NPs, which can be shown by quantum chemistry calculations. The number of hydrogen bonds between two ZnO crystal slabs were calculated, which was found to decrease with increasing the number of surface methoxyl groups (Figure S4e). For $Zn_{13}O_{33}H_{33}$ where the surface is fully covered by −OH groups, the interface consists of 11 hydrogen bonds (Figure S4a), providing a total binding energy of *ca.* 231 kJ/mol. We further performed an all atom MD simulation using the package GROMACS[79] based on GMX force field under rectangular periodic boundary conditions, which allows us to consider the contribution of water molecules for promoting the formation of chains. A network of hydrogen bonds was found in all the area (Figure 3a). Especially, we found that water molecules can bridge NPs by connecting the surface O and H atoms through hydrogen bonding (Figure 3b). However, such observation does not mean hydrogen bonds between NPs are anisotropic. The formation of 1D assemblies is in fact a result of cooperative interparticle forces mainly including hydrogen bonding and dipolar interactions. Here, dipole−dipole attraction triggers the anisotropic assembly and hydrogen bonds between NPs make chains thermodynamically stable. In other words, once ZnO NPs align with each other due to the presence of dipole moment, hydrogen bonds are important to hold them in position. When NPs approach even closer under a net attractive force, the direct hydrogen bonds between two NPs can take effect for further stabilization of the structure (Figure S4).

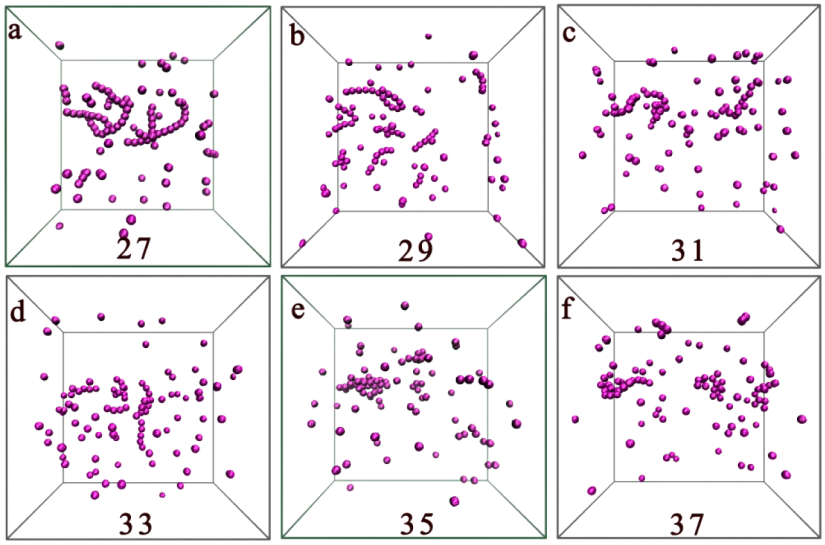

Figure 4. Self-assembled structures of ZnO NPs under equilibrium with different interaction parameters (27−37) obtained from DPD simulations. Solvent beads are not shown for clarity.

To further understand the influence of NP-solvent interactions on the self-assembly of ZnO NPs, we then performed DPD simulations using the package GALAMOST[80,81] based on rigid body model.[82] We noted that during the synthesis, besides a transparent dispersion of colloidal ZnO NPs, a large amount of white precipitates will be consistently obtained. XRD pattern confirmed that they are consisted of ZnO NPs (Figure S5a), which can be however readily dispersed into water (Figure S5b). Such finding indicated that ZnO NPs is solvophilic for water, however, is relatively solvophobic for methanol. The reason for the limited solubility in methanol may be due to the presence of surface methoxyl groups, which largely reduce the possibility of forming hydrogen bonding with solvent molecules. We therefore assigned interaction parameters (IP) of 27 to describe the interactions between ZnO NPs with water and increased IP gradually until 37 to investigate the effect of NP-solvent interactions on the self-assembly process. Here a larger IP means a higher solvophobicity, which more likely reflects the interactions between ZnO NPs and methanol. Same dipole moment was used for different solvent conditions due to the minimal influence of surface groups on the electric dipole moment of ZnO NPs confirmed by our quantum mechanical calculations (Figure S6). The corresponding results were summarized (Figure 4). It was found that long chain-like structures can form in water (IP of 27) (Figure 4a), which matches well with experimental observations (Figure 1). However, when IP was increased, the formation of anisotropic assemblies was not favored (Figure 4) and at IPs of 35 and 37, no distinct 1D assembly can be observed (Figure 4e-f). Overall, our DPD simulations indicated that solvophilic interactions which originated from hydrogen bonding are essential for the formation of long chains, whereas, solvophobic interactions may disturb the dipolar attraction.

Finally, we investigated the energy transfer (ET) between ZnO NPs in the chain-like structures. The study on ET is usually focused on the exciton emission due to its narrow width with tunable characteristic and the well-defined Stroke-shift. Compared with the extensive work on small band gap NP assemblies, the investigations on ET in nanoassemblies of ZnO nanostructures are sparse. For ZnO quantum dots, the short exciton radiative lifetime around tens of picoseconds[83] can pose challenge on the probing of even shorter lifetime when proper environment is present for ET. Also, the high surface-to-volume ratio of ZnO nanostructures usually diminishes the intensity of ultraviolet emission with increased concentration of surface defects.[78] Indeed, for ZnO nanostructures, besides the emission resulted from radiative exciton recombination, the presence of defect related energy levels were suggested to be responsible for the visible emission with much longer lifetime (in the order of several ns).[83] As ZnO NP chains in our study have dominant defect-related emission (Figure 2), the probing of visible emission will be more practical and relevant to the major ET process.

To eliminate the influence of solvents, we investigated the change of optical properties along with the growth of chains in water. The size of chains increased from hundreds of nanometers to micrometers as indicated by dynamic light scattering (DLS) (Table 1) and TEM imaging (Figure 5) when the aging time varied from 1 day to 6 days. The growth of chains followed a branching mechanism; *i.e.*, longer chains with more branches formed upon more aging time. Especially, the emergence of chain networks can be found after aging for 6 days (Figure 5c,d). The emission intensity decrease may indicate the existence of Förster resonance energy transfer (FRET) in highly branched chains (Figure 6b). As the absorption spectra (Figure 6a)

TABLE 1. Summary of Sizes Determined by DLS and Lifetimes for Chain-Like Structures Obtained after Different Aging Time

aging time (days)	1	3	6
DLS sizes	100 nm	300 nm	1 μm
lifetime (ns)	16.31 $\pm$ 0.44 (22.44%)	15.41 $\pm$ 0.45(22.44%)	5.88 $\pm$ 0.20 (16.18%)
	146.80 $\pm$ 6.52 (77.56%)	132.20 $\pm$ 5.44 (77.56%)	76.13 $\pm$ 1.56 (83.82%)

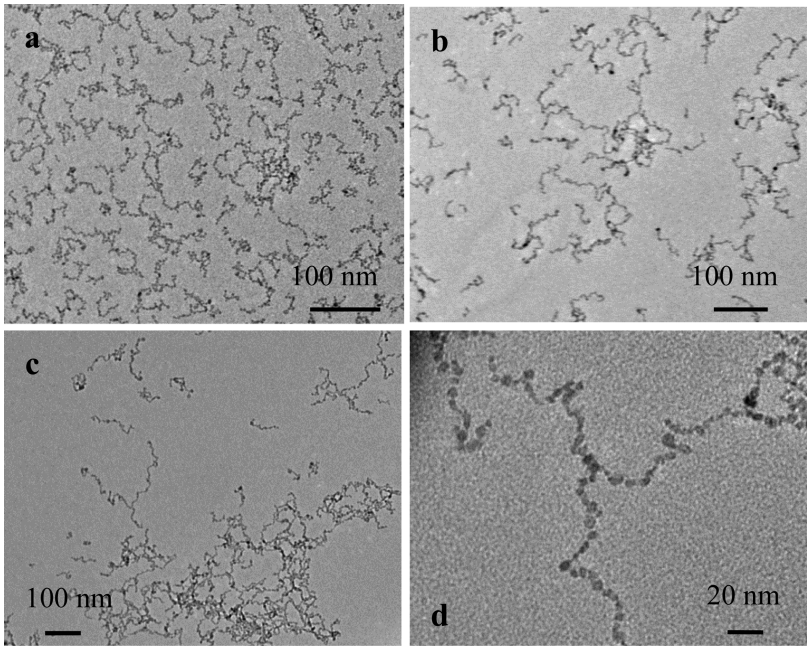

Figure 5. TEM images of ZnO chain-like structures obtained after (a) 1 day, (b) 3 days and (c) 6 days aging. (d) TEM images of a typical branch.

showed a maximum at *ca.* 337 nm with no obvious shift after different durations of aging, electron delocalization (Dexter transfer)[55] does not likely play a significant role here. A red-shift of the maximum emission from 550 to 564 nm (Figure 6b) is another indication for the existence of FRET considering the size-dependent nature of visible emission.[78,84] The time-dependent intensity decays fitted with a two-exponential decay function[85] clearly showed that the lifetime of both fast and slow component decreased when the size of chains increased (Table 1 and Figure 6c). The lifetimes for NPs in methanol is much longer, 32.76 ns for fast component and 1.28 μs for slow component (Figure S7), which may imply that the kinetic parameters in Table 1 are already altered lifetimes due to electronic energy transfer. The short component describes dynamics of the luminescence in smaller particles. The drastic reduction of its lifetime is due to enhanced FRET quenching of smaller particles, which becomes more efficient when the chain networks are formed (*vide infra*). The longer component is typically attributed to the native radiative lifetime of the largest NPs in the ensemble. We suggested that the decrease of longer component is likely a result of the greater statistical probability to find even bigger neighboring NPs in the chains.[85]

We note that, essentially, the ET mechanism here is still based on the overlap of exciton emission and absorption (Figure 6d). Here, the correlation of visible emission with the transition of excited electrons from conduction band (CB) to deep acceptor levels makes its coupling with ET process possible (Figure S8). NPs of relatively bigger diameters serve as exciton acceptors due to a narrower band gap and relatively smaller NPs serve as donors. When FRET occurs, the excitation will be concentrated on bigger NPs, which can be energy sinks in the chains. Presumably, an emission enhancement from these bigger NPs would be observed besides the quenching (Figure 6b). However, there are two possible facts making it hard to achieve: first, the broad size distribution of NPs may blur the spectral separation of emission for different sized NPs, which may be seen from the nearly unchanged half-width of emission peaks accompanying the quenching (Figure 6b). Second, the percentage of these bigger NPs with a diameter significantly above average is very low, making the dominant emission from them still weaker than that from smaller ones after quenching; as a result, the possible enhancement may be obscured by the emission quenching of smaller NPs. Similar observation has been found in CdTe NP chains.[85]

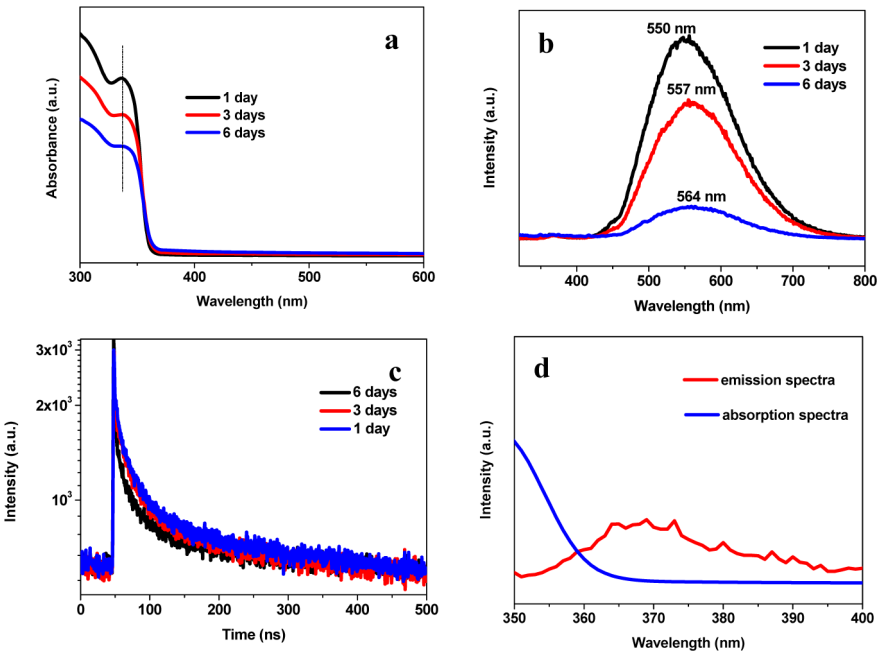

Figure 6. (a) UV spectra, (b) steady-state PL spectra and (c) transient PL spectra of ZnO NP assemblies obtained at different time. The excitation wavelength is 320 nm and the emission at 550 nm was probed. (d) The overlap of emission and absorption of ZnO NP assemblies after a 3-day aging.

It is suggested that FRET efficiency (E) can be described as

$$E = \frac{N(R_0)^6}{N(R^0)^6 + r^6}$$

$$(R_0)^6 = \text{constant} \times \kappa^2 \times \Phi_D \times J(\lambda) \times n^{-4}$$

where N is the average number of acceptor NPs interacting with one donor, r is the distance between donor and acceptor NPs, R_0 is the separation distance that yields 50% energy transfer efficiency, κ^2 is directional relationship of transition dipoles, Φ_D is the quantum yield of the donor, $J(\lambda)$ is the spectral overlap of donor and acceptor, and n is the refractive index of the medium. According to our observation, the branching of ZnO NPs in chains is the main mechanism for the growth of chain network (Figure 5). We believe the branching of chains can enhance the efficiency of FRET by increasing N: first, NPs positioned at the branched points (Figure 5d) will obviously have more neighbors, serving as a joint connection for multiple ET channels; second, the staggered network also allows NPs in other positions to find more partners in some vicinity. Similar with previously reported CdTe NP chains,[85] here FRET is also improved by the short interparticle distance and the alignment of particle lattices. We noted that for chains after 1-day and 3-day aging, the decrease of longer component is more obvious than the shorter one, which could be due to the fact that the branching occurs initially from larger NPs due to their intrinsic greater electric dipole moment. The percentage of decrease for fast component upon the growth of chains (61.3%) is even larger than that of the formation of CdTe chains as against individual NPs (41.9%),[85] which can be attributed to the formation of larger network-like ensembles.

We would also like to compare our system with metallic NP chains, which has been suggested to be waveguides under the diffraction limit. In our cases, the branching of chain-like structures improves the FRET efficiency by providing multiple ET channels. However, it has been shown that the bent structures reminiscent of simple branches will decrease the ET efficiency in metallic NP chains due to the energy conversion from propagating modes to free radiation.[86] Such difference can be attributed to the different ET mechanisms which involve excitons and plasmon polarons, respectively. It may be possible to harness the energy loss in bent metallic nanostructures through the enhancement of FRET.[87]

CONCLUSIONS

The spontaneous formation of long ZnO NP chains was observed in water. The size of chains was found to increase upon aging by a branching mechanism, which finally led to the formation of chain networks. Quantum mechanical calculations, MD and DPD simulations highlighted the importance of NP-solvent interactions especially hydrogen bonding in stabilizing the chain-like structure. Energy transfer in 1D close spaced assemblies was observed by probing the variation of dominant visible emission. The presence of multiple energy transfer channels in chain networks strongly improved the FRET quenching

efficiency. The demonstration of hydrogen bonding for promoting anisotropic self-assembly of inorganic NPs may provide new insight into the design of functional superstructures. The enhanced energy transfer rate in branched semiconductor NP chains may be coupled with multimodal plasmonics.

EXPERIMENTAL SECTION

Synthesis. ZnO NPs were prepared as follows: 0.979 g of $Zn(Ac)_2 \cdot 2H_2O$ (4.46 mmol) and 100 μL of water were added into a round flask containing 42 mL of methanol. The solution was heated to 60 °C with magnetic stirring until all the materials were dissolved. 0.4859 g of KOH (7.22 mmol) was added into 23 mL of methanol, which was then dissolved by ultrasonication and poured into the flask. The solution turned milky immediately the base solution was added, but became transparent a few minutes later. At a constant temperature of 60 °C, the system was heated for 2 h. The synthesis will produce a transparent dispersion of ZnO NPs in methanol along with white precipitates. To prepare aqueous dispersion of ZnO NPs, methanol was removed by rotary evaporation at 30 °C. The remaining was immediately dispersed in the same amount of water. For the growth of ZnO NP chains, the aqueous dispersion was kept at 4 °C for different durations (1, 3, and 6 days).

Characterization. For TEM observation, one drop of methanol or aqueous dispersion of ZnO NPs was added to the surface of copper grids with carbon holey film which was placed upon a piece of filter paper. The grids were ready for use after complete drying. A transmission electron microscope (Tecnai G2 F20 S-Twin with 200 kV accelerating voltage of electron beam) was used to acquire TEM images. To obtain UV−vis spectra, a U4100 UV− vis−NIR spectrometer (Hitachi, Japan) was used to characterize the absorption properties of methanol and aqueous dispersion of ZnO NPs in a quartz cuvette. The photoluminescence spectra were measured using a Fluoromax-4 fluorescence spectrophotometer (HORIBA Jobin Yvon, Japan) with an excitation wavelength at 320 nm. Time-resolved photoluminescence spectra were measured on an FL920-Fluorescence Lifetime Spectrometer (Edinburgh Instruments) with MCP-PMT. For Fourier transform infrared (FT-IR) spectra, a PerkinElmer spectrum frontier optical spectrometer was used and the samples were pressed with KBr pellets and dried before measurement. X-ray photoelectron spectroscopy (XPS) was performed using PHI ESCA 5700 with Al Kα (1486.6 eV). Sputtering by Ar^+ under 1 μA and 300 eV for 2 min was used before the test to ensure an accurate data. X-ray diffraction (XRD) measurements were performed on X'Pert-Pro (Philips) using Cu Kα (λ = 0.1541 nm) generated at 40 kV and 100 mA. A scanning speed of 0.2° per min was used.

Quantum Mechanical Calculation. *1. Calculation of the Number of Hydrogen Bonds.* For this purpose, we created a slab of ZnO crystal structure ($Zn_{13}O_{33}H_{33}$) built along *c*-axis. We also built several atomistic structures by replacing H atoms with methoxyl groups to mimic the condition in methanol (Figure S4). Two identical slabs were placed by changing the coordinate along one axis. The distance between zinc atoms in different slabs was set to be 0.45 nm, which is the spacing in the order of lattice constants. The structure optimization was done by freezing the heavy atoms and allowing H and C atoms to relax under Merck molecular force field.

2. Calculation of Dipole Moment. We first built an atomistic model of ZnO NPs ($Zn_{18}O_{39}C_{35}H_{105}$) according to the hexagonal crystal structure, assuming that most of the crystal planes are more inert O-terminated surfaces (Figure S6c). This model can reasonably reflect the surface state of ZnO NPs in methanol as the exposed oxygen atoms are all connected with $-CH_3$ groups. A similar model ($Zn_{18}O_{39}H_{35}$) was also built by replacing all $-CH_3$ groups with H atoms, which mimic the hydrolysis process when ZnO NPs are dispersed in water (Figure S6a). The resultant atomistic model with surface −OH groups therefore corresponds to the structure of ZnO NPs in water. Merck molecular force field (MMFF) was used to optimize the geometries of these atomic models with zinc and oxygen atoms positioned in the crystal lattice freezing. This process allowed all bonds to acquire a relaxed configuration. Single point energy mode was then employed to compute electric dipole moment of the equilibrium atomic model using the semiempirical parameter model 3 (PM3) methods. The discussions about the calculation results can be found in the Supporting Information.

MD Simulation. Newton's equations of motion are integrated using the leapfrog algorithm with time step of 0.5 fs and the total simulation time is 10 ns. The bond lengths are constrained using the LINCS algorithm with a relative geometric tolerance of 10^{-4} and the nonbonded interactions including Particle Mesh Ewald (PME) electrostatics are truncated at a distance of 1.2 nm. The atomistic model of ZnO NPs ($Zn_{42}O_{78}H_{39}$) was built with terminated −OH groups and the distance between two NPs was set to be 0.45 nm (Figure S9), which allows several water molecules to exist in between the NPs.

DPD Simulations. In our DPD simulations, we used reduced units and assumed all coarse-grained (CG) beads are equal on volume. The bead diameter, bead mass and the temperature were set to be unity and the total simulation steps are 1×10^5. We set the box side length as $40 \times 40 \times 20$ and controlled the number density of CG beads at 3, so the total number of beads in our simulations is 96 000. It contains 100 C_{120} NPs, in which 120 CG beads form a rigid body. The remaining part represents solvent molecules (84 000 beads). To mimic electric dipole moment on each NP, 12 negative charges and 12 positive charges were given on the two pole regions of each NP, respectively. This charge model is derived from quantum chemistry calculation (Figure S6), which shows similar charge distributions (Figure S6). Particle−particle-particle-mesh (PPPM) Ewald summation method was used to calculate the long-range electrostatic interactions.[88] We fixed the interaction parameter (IP) between the same types of beads at 25 to correctly describe the compressibility of solvents. The IPs between ZnO NPs and different solvents, which reflect the NP-solvent interactions (van der Waals forces, hydrogen bonding and solvophobic interaction) are critical factors in our DPD simulations. Even though there is no available literature data for us to use, we can set relative IPs according to the experimental observation. Here, the difference of IPs is more important than their actual value. All DPD simulations were performed in NVT ensemble on Nvidia Tesla C2050 GPU. More details about DPD simulations can be found in the Supporting Information.

Conflict of Interest: The authors declare no competing financial interest.

Acknowledgment. M.Y. would like to thank the financial support from the National Natural Science Foundation of China (Grant No. 21303032), Technology Foundation for Selected Overseas Chinese Scholar, Ministry of Human Resources and Social Security of China (Grant No. AUWQ1660010214), China Postdoctoral Science Foundation (Grant No. 2014M550184), Heilongjiang Postdoctoral Science Foundation (Grant No. LBH-Q13074), HIT Young Talent Program (Grant No. AUGA5710050613) and Fundamental Research Funds for the Central Universities (Grant No. HIT. IBRSEM. A. 201406); M.Y. would also like to thank Prof. Guangsheng Pang from Jilin University for his kind help in acquiring the transient PL spectra; Y.H. would like to thank the financial support from HIT 100-talent program (Grant No. AUGA5710006813) and Fundamental Research Funds for the Central Universities (Grant No. HIT IBRSEM. A. 201405); J.Z. would like to thank the financial support from the National Natural Science Foundation of China (Grant No. 51222205); J.H. would like to thank the financial support from the National Natural Science Foundation of China (Grant No. 11421091); Z.L. would like to thank the financial support from Jilin Province Science and Technology Development Plan (20140519004JH).

Supporting Information Available: TEM images of ZnO NPs in methanol; IR and XPS spectra of ZnO NPs obtained from water and methanol; the results of quantum mechanical calculations for interparticle hydrogen bonds; XRD pattern of white precipitates obtained from the synthesis and optical images of white precipitates in methanol and water; the results of the calculations of dipole moment and the corresponding discussions; transient PL spectra for ZnO NPs in methanol; schematic illustration of FRET involving defect-related energy level; the assignment of the distance between two NPs in MD simulations; the details for dissipative particle dynamics. The Supporting Information is available free of charge on the ACS Publications website at DOI: 10.1021/acsnano.5b00344.

REFERENCES AND NOTES

1. Park, J.; Joo, J.; Kwon, S. G.; Jang, Y.; Hyeon, T. Synthesis of Monodisperse Spherical Nanocrystals. *Angew. Chem., Int. Ed.* **2007**, *46*, 4630–4660.
2. Daniel, M. C.; Astruc, D. Gold Nanoparticles: Assembly, Supramolecular Chemistry, Quantum-Size-Related Properties, and Applications toward Biology, Catalysis, and Nanotechnology. *Chem. Rev.* **2004**, *104*, 293–346.
3. Liz-Marzan, L. M. Tailoring Surface Plasmons through the Morphology and Assembly of Metal Nanoparticles. *Langmuir* **2006**, *22*, 32–41.
4. Kotov, N. A.; Winter, J. O.; Clements, I. P.; Jan, E.; Timko, B. P.; Campidelli, S.; Pathak, S.; Mazzatenta, A.; Lieber, C. M.; Prato, M.; Bellamkonda, R. V.; Silva, G. A.; Kam, N. W. S.; Patolsky, F.; Ballerini, L. Nanomaterials for Neural Interfaces. *Adv. Mater.* **2009**, *21*, 3970–4004.
5. Lu, A. H.; Salabas, E. L.; Schuth, F. Magnetic Nanoparticles: Synthesis, Protection, Functionalization, and Application. *Angew. Chem., Int. Ed.* **2007**, *46*, 1222–1244.
6. Chen, C.; Kang, Y. J.; Huo, Z. Y.; Zhu, Z. W.; Huang, W. Y.; Xin, H. L. L.; Snyder, J. D.; Li, D. G.; Herron, J. A.; Mavrikakis, M.; Chi, M. F.; More, K. L.; Li, Y. D.; Markovic, N. M.; Somorjai, G. A.; Yang, P. D.; Stamenkovic, V. R. Highly Crystalline Multimetallic Nanoframes with Three-Dimensional Electrocatalytic Surfaces. *Science* **2014**, *343*, 1339–1343.
7. Shan, Z. W.; Adesso, G.; Cabot, A.; Sherburne, M. P.; Asif, S. A. S.; Warren, O. L.; Chrzan, D. C.; Minor, A. M.; Alivisatos, A. P. Ultrahigh Stress and Strain in Hierarchically Structured Hollow Nanoparticles. *Nat. Mater.* **2008**, *7*, 947–952.
8. Kotov, N. A. Inorganic Nanoparticles as Protein Mimics. *Science* **2010**, *330*, 188–189.
9. Tang, Z. Y.; Kotov, N. A.; Giersig, M. Spontaneous Organization of Single CdTe Nanoparticles into Luminescent Nanowires. *Science* **2002**, *297*, 237–240.
10. Tang, Z. Y.; Zhang, Z. L.; Wang, Y.; Glotzer, S. C.; Kotov, N. A. Self-Assembly of CdTe Nanocrystals into Free-Floating Sheets. *Science* **2006**, *314*, 274–278.
11. Talapin, D. V.; Shevchenko, E. V.; Murray, C. B.; Kornowski, A.; Forster, S.; Weller, H. CdSe and CdSe/CdS Nanorod Solids. *J. Am. Chem. Soc.* **2004**, *126*, 12984–12988.
12. Bishop, K. J. M.; Wilmer, C. E.; Soh, S.; Grzybowski, B. A. Nanoscale Forces and Their Uses in Self-Assembly. *Small* **2009**, *5*, 1600–1630.
13. Shevchenko, E. V.; Talapin, D. V.; Kotov, N. A.; O'Brien, S.; Murray, C. B. Structural Diversity in Binary Nanoparticle Superlattices. *Nature* **2006**, *439*, 55–59.
14. Zhuang, Z. B.; Peng, Q.; Zhang, B.; Li, Y. D. Controllable Synthesis of Cu_2S Nanocrystals and Their Assembly into a Superlattice. *J. Am. Chem. Soc.* **2008**, *130*, 10482–10483.
15. Wang, T.; Zhuang, J. Q.; Lynch, J.; Chen, O.; Wang, Z. L.; Wang, X. R.; LaMontagne, D.; Wu, H. M.; Wang, Z. W.; Cao, Y. C. Self-Assembled Colloidal Superparticles from Nanorods. *Science* **2012**, *338*, 358–363.
16. Tang, Z. Y.; Kotov, N. A. One-Dimensional Assemblies of Nanoparticles: Preparation, Properties, and Promise. *Adv. Mater.* **2005**, *17*, 951–962.
17. Han, X. G.; Liu, Y. D.; Yin, Y. D. Colorimetric Stress Memory Sensor Based on Disassembly of Gold Nanoparticle Chains. *Nano Lett.* **2014**, *14*, 2466–2470.
18. Gao, B.; Arya, G.; Tao, A. R. Self-Orienting Nanocubes for the Assembly of Plasmonic Nanojunctions. *Nat. Nanotechnol.* **2012**, *7*, 433–437.
19. Barrow, S. J.; Rossouw, D.; Funston, A. M.; Botton, G. A.; Mulvaney, P. Mapping Bright and Dark Modes in Gold Nanoparticle Chains Using Electron Energy Loss Spectroscopy. *Nano Lett.* **2014**, *14*, 3799–3808.
20. Sanchot, A.; Baffou, G.; Marty, R.; Arbouet, A.; Quidant, R.; Girard, C.; Dujardin, E. Plasmonic Nanoparticle Networks for Light and Heat Concentration. *ACS Nano* **2012**, *6*, 3434–3440.
21. Teulle, A.; Bosman, M.; Girard, C.; Gurunatha, K. L.; Li, M.; Mann, S.; Dujardin, E. Multimodal Plasmonics in Fused Colloidal Networks. *Nat. Mater.* **2015**, *14*, 87–94.
22. Torimoto, T.; Yamashita, M.; Kuwabata, S.; Sakata, T.; Mori, H.; Yoneyama, H. Fabrication of CdS Nanoparticle Chains Along DNA Double Strands. *J. Phys. Chem. B* **1999**, *103*, 8799–8803.
23. Yin, Y. D.; Xia, Y. N. Self-Assembly of Spherical Colloids into Helical Chains with Well-Controlled Handedness. *J. Am. Chem. Soc.* **2003**, *125*, 2048–2049.
24. Shen, X. S.; Chen, L. Y.; Li, D. H.; Zhu, L. F.; Wang, H.; Liu, C. C.; Wang, Y.; Xiong, Q. H.; Chen, H. Y. Assembly of Colloidal Nanoparticles Directed by the Microstructures of Polycrystalline Ice. *ACS Nano* **2011**, *5*, 8426–8433.
25. Gao, M. R.; Zhang, S. R.; Xu, Y. F.; Zheng, Y. R.; Jiang, J.; Yu, S. H. Self-Assembled Platinum Nanochain Networks Driven by Induced Magnetic Dipoles. *Adv. Funct. Mater.* **2014**, *24*, 916–924.
26. Singh, G.; Chan, H.; Baskin, A.; Gelman, E.; Repnin, N.; Kral, P.; Klajn, R. Self-Assembly of Magnetite Nanocubes into Helical Superstructures. *Science* **2014**, *345*, 1149–1153.
27. Keng, P. Y.; Shim, I.; Korth, B. D.; Douglas, J. F.; Pyun, J. Synthesis and Self-Assembly of Polymer-Coated Ferromagnetic Nanoparticles. *ACS Nano* **2007**, *1*, 279–292.
28. Nakata, K.; Hu, Y.; Uzun, O.; Bakr, O.; Stellacci, F. Chains of Superparamagnetic Nanoplarticles. *Adv. Mater.* **2008**, *20*, 4294–4299.
29. Liu, K.; Nie, Z. H.; Zhao, N. N.; Li, W.; Rubinstein, M.; Kumacheva, E. Step-Growth Polymerization of Inorganic Nanoparticles. *Science* **2010**, *329*, 197–200.
30. Nie, Z. H.; Fava, D.; Kumacheva, E.; Zou, S.; Walker, G. C.; Rubinstein, M. Self-Assembly of Metal-Polymer Analogues of Amphiphilic Triblock Copolymers. *Nat. Mater.* **2007**, *6*, 609–614.
31. Wang, H.; Chen, L. Y.; Shen, X. S.; Zhu, L. F.; He, J. T.; Chen, H. Y. Unconventional Chain-Growth Mode in the Assembly of Colloidal Gold Nanoparticles. *Angew. Chem., Int. Ed.* **2012**, *51*, 8021–8025.
32. Caswell, K. K.; Wilson, J. N.; Bunz, U. H. F.; Murphy, C. J. Preferential End-to-End Assembly of Gold Nanorods by Biotin-Streptavidin Connectors. *J. Am. Chem. Soc.* **2003**, *125*, 13914–13915.
33. Chen, Q.; Whitmer, J. K.; Jiang, S.; Bae, S. C.; Luijten, E.; Granick, S. Supracolloidal Reaction Kinetics of Janus Spheres. *Science* **2011**, *331*, 199–202.
34. Ding, B. Q.; Deng, Z. T.; Yan, H.; Cabrini, S.; Zuckermann, R. N.; Bokor, J. Gold Nanoparticle Self-Similar Chain Structure Organized by DNA Origami. *J. Am. Chem. Soc.* **2010**, *132*, 3248–3249.
35. Lee, H. Y.; Shin, S. H. R.; Drews, A. M.; Chirsan, A. M.; Lewis, S. A.; Bishop, K. J. M. Self-Assembly of Nanoparticle Amphiphiles with Adaptive Surface Chemistry. *ACS Nano* **2014**, *8*, 9979–9987.
36. DeVries, G. A.; Brunnbauer, M.; Hu, Y.; Jackson, A. M.; Long, B.; Neltner, B. T.; Uzun, O.; Wunsch, B. H.; Stellacci, F. Divalent Metal Nanoparticles. *Science* **2007**, *315*, 358–361.
37. Miszta, K.; de Graaf, J.; Bertoni, G.; Dorfs, D.; Brescia, R.; Marras, S.; Ceseracciu, L.; Cingolani, R.; van Roij, R.; Dijkstra, M.; Manna, L. Hierarchical Self-Assembly of Suspended Branched Colloidal Nanocrystals into Superlattice Structures. *Nat. Mater.* **2011**, *10*, 872–876.
38. Gibaud, T.; Barry, E.; Zakhary, M. J.; Henglin, M.; Ward, A.; Yang, Y. S.; Berciu, C.; Oldenbourg, R.; Hagan, M. F.; Nicastro,

D.; Meyer, R. B.; Dogic, Z. Reconfigurable Self-Assembly through Chiral Control of Interfacial Tension. *Nature* **2012**, *481*, 348–351.
39. Walker, D. A.; Leitsch, E. K.; Nap, R. J.; Szleifer, I.; Grzybowski, B. A. Geometric Curvature Controls the Chemical Patchiness and Self-Assembly of Nanoparticles. *Nat. Nanotechnol.* **2013**, *8*, 676–681.
40. Pacholski, C.; Kornowski, A.; Weller, H. Self-Assembly of ZnO: From Nanodots, to Nanorods. *Angew. Chem., Int. Ed.* **2002**, *41*, 1188–1191.
41. Sinyagin, A. Y.; Belov, A.; Tang, Z. N.; Kotov, N. A. Monte Carlo Computer Simulation of Chain Formation from Nanoparticles. *J. Phys. Chem. B* **2006**, *110*, 7500–7507.
42. Zhang, Z. L.; Tang, Z. Y.; Kotov, N. A.; Glotzer, S. C. Simulations and Analysis of Self-Assembly of CdTe Nanoparticles into Wires and Sheets. *Nano Lett.* **2007**, *7*, 1670–1675.
43. Yang, M.; Sun, K.; Kotov, N. A. Formation and Assembly-Disassembly Processes of ZnO Hexagonal Pyramids Driven by Dipolar and Excluded Volume Interactions. *J. Am. Chem. Soc.* **2010**, *132*, 1860–1872.
44. Li, P.; Wei, Z.; Wu, T.; Peng, Q.; Li, Y. D. Au-ZnO Hybrid Nanopyramids and Their Photocatalytic Properties. *J. Am. Chem. Soc.* **2011**, *133*, 5660–5663.
45. Choi, S. H.; Kim, E. G.; Park, J.; An, K.; Lee, N.; Kim, S. C.; Hyeon, T. Large-Scale Synthesis of Hexagonal Pyramid-Shaped ZnO Nanocrystals from Thermolysis of Zn-Oleate Complex. *J. Phys. Chem. B* **2005**, *109*, 14792–14794.
46. Zhang, S. G. Fabrication of Novel Biomaterials through Molecular Self-Assembly. *Nat. Biotechnol.* **2003**, *21*, 1171–1178.
47. Song, B.; Wei, H.; Wang, Z. Q.; Zhang, X.; Smet, M.; Dehaen, W. Supramolecular Nanofibers by Self-Organization of Bola-Amphiphiles through a Combination of Hydrogen Bonding and Pi-Pi Stacking Interactions. *Adv. Mater.* **2007**, *19*, 416–420.
48. Han, S. Y.; Cao, S. S.; Wang, Y. M.; Wang, J. Q.; Xia, D. H.; Xu, H.; Zhao, X. B.; Lu, J. R. Self-Assembly of Short Peptide Amphiphiles: The Cooperative Effect of Hydrophobic Interaction and Hydrogen Bonding. *Chem.-Eur. J.* **2011**, *17*, 13095–13102.
49. Yoo, S. I.; Yang, M.; Brender, J. R.; Subramanian, V.; Sun, K.; Joo, N. E.; Jeong, S. H.; Ramamoorthy, A.; Kotov, N. A. Inhibition of Amyloid Peptide Fibrillation by Inorganic Nanoparticles: Functional Similarities with Proteins. *Angew. Chem., Int. Ed.* **2011**, *50*, 5110–5115.
50. Murray, C. B.; Kagan, C. R.; Bawendi, M. G. Self-Organization of CdSe Nanocrystallites into 3-Dimensional Quantum-Dot Superlattices. *Science* **1995**, *270*, 1335–1338.
51. Talapin, D. V.; Murray, C. B. PbSe Nanocrystal Solids for N- and P-Channel Thin Film Field-Effect Transistors. *Science* **2005**, *310*, 86–89.
52. Crooker, S. A.; Hollingsworth, J. A.; Tretiak, S.; Klimov, V. I. Spectrally Resolved Dynamics of Energy Transfer in Quantum-Dot Assemblies: Towards Engineered Energy Flows in Artificial Materials. *Phys. Rev. Lett.* **2002**, *89*, 186802.
53. Kagan, C. R.; Murray, C. B.; Nirmal, M.; Bawendi, M. G. Electronic Energy Transfer in CdSe Quantum Dot Solids. *Phys. Rev. Lett.* **1996**, *76*, 1517–1520.
54. Wargnier, R.; Baranov, A. V.; Maslov, V. G.; Stsiapura, V.; Artemyev, M.; Pluot, M.; Sukhanova, A.; Nabiev, I. Energy Transfer in Aqueous Solutions of Oppositely Charged CdSe/ZnS Core/Shell Quantum Dots and in Quantum Dot-Nanogold Assemblies. *Nano Lett.* **2004**, *4*, 451–457.
55. Koole, R.; Liljeroth, P.; Donega, C. D.; Vanmaekelbergh, D.; Meijerink, A. Electronic Coupling and Exciton Energy Transfer in CdTe Quantum-Dot Molecules. *J. Am. Chem. Soc.* **2006**, *128*, 10436–10441.
56. Micic, O. I.; Jones, K. M.; Cahill, A.; Nozik, A. J. Optical, Electronic, and Structural Properties of Uncoupled and Close-Packed Arrays of InP Quantum Dots. *J. Phys. Chem. B* **1998**, *102*, 9791–9796.
57. Tian, Z. R. R.; Voigt, J. A.; Liu, J.; McKenzie, B.; McDermott, M. J.; Rodriguez, M. A.; Konishi, H.; Xu, H. F. Complex and Oriented ZnO Nanostructures. *Nat. Mater.* **2003**, *2*, 821–826.
58. Law, M.; Greene, L. E.; Johnson, J. C.; Saykally, R.; Yang, P. D. Nanowire Dye-Sensitized Solar Cells. *Nat. Mater.* **2005**, *4*, 455–459.
59. Wang, X. D.; Summers, C. J.; Wang, Z. L. Large-Scale Hexagonal-Patterned Growth of Aligned ZnO Nanorods for Nano-Optoelectronics and Nanosensor Arrays. *Nano Lett.* **2004**, *4*, 423–426.
60. Huang, M. H.; Mao, S.; Feick, H.; Yan, H. Q.; Wu, Y. Y.; Kind, H.; Weber, E.; Russo, R.; Yang, P. D. Room-Temperature Ultraviolet Nanowire Nanolasers. *Science* **2001**, *292*, 1897–1899.
61. Wang, Z. L. Piezopotential Gated Nanowire Devices: Piezotronics and Piezo-Phototronics. *Nano Today* **2010**, *5*, 540–552.
62. Xu, S.; Wang, Z. L. One-Dimensional ZnO Nanostructures: Solution Growth and Functional Properties. *Nano Res.* **2011**, *4*, 1013–1098.
63. Liu, B.; Zeng, H. C. Hydrothermal Synthesis of ZnO Nanorods in the Diameter Regime of 50 nm. *J. Am. Chem. Soc.* **2003**, *125*, 4430–4431.
64. Liu, B.; Zeng, H. C. Fabrication of ZnO "Dandelions" *via* a Modified Kirkendall Process. *J. Am. Chem. Soc.* **2004**, *126*, 16744–16746.
65. Zhang, H.; Wang, D. Y. Controlling the Growth of Charged-Nanoparticle Chains through Interparticle Electrostatic Repulsion. *Angew. Chem., Int. Ed.* **2008**, *47*, 3984–3987.
66. Li, M.; Johnson, S.; Guo, H. T.; Dujardin, E.; Mann, S. A Generalized Mechanism for Ligand-Induced Dipolar Assembly of Plasmonic Gold Nanoparticle Chain Networks. *Adv. Funct. Mater.* **2011**, *21*, 851–859.
67. Zhang, H.; Fung, K. H.; Hartmann, J.; Chan, C. T.; Wang, D. Y. Controlled Chainlike Agglomeration of Charged Gold Nanoparticles *via* a Deliberate Interaction Balance. *J. Phys. Chem. C* **2008**, *112*, 16830–16839.
68. Shanbhag, S.; Kotov, N. A. On the Origin of a Permanent Dipole Moment in Nanocrystals with a Cubic Crystal Lattice: Effects of Truncation, Stabilizers, and Medium for CdS Tetrahedral Homologues. *J. Phys. Chem. B* **2006**, *110*, 12211–12217.
69. Sanchez-Iglesias, A.; Grzelczak, M.; Altantzis, T.; Goris, B.; Perez-Juste, J.; Bals, S.; Van Tendeloo, G.; Donaldson, S. H.; Chmelka, B. F.; Israelachvili, J. N.; Liz-Marzan, L. M. Hydrophobic Interactions Modulate Self-Assembly of Nanoparticles. *ACS Nano* **2012**, *6*, 11059–11065.
70. Choueiri, R. M.; Klinkova, A.; Therien-Aubin, H.; Rubinstein, M.; Kumacheva, E. Structural Transitions in Nanoparticle Assemblies Governed by Competing Nanoscale Forces. *J. Am. Chem. Soc.* **2013**, *135*, 10262–10265.
71. He, J.; Huang, X. L.; Li, Y. C.; Liu, Y. J.; Babu, T.; Aronova, M. A.; Wang, S. J.; Lu, Z. Y.; Chen, X. Y.; Nie, Z. H. Self-Assembly of Amphiphilic Plasmonic Micelle-Like Nanoparticles in Selective Solvents. *J. Am. Chem. Soc.* **2013**, *135*, 7974–7984.
72. Spitz, R. N.; Barton, J. E.; Barteau, M. A.; Staley, R. H.; Sleight, A. W. Characterization of the Surface Acid-Base Properties of Metal-Oxides by Titration Displacement-Reactions. *J. Phys. Chem.* **1986**, *90*, 4067–4075.
73. Au, C. T.; Hirsch, W.; Hirschwald, W. Adsorption and Interaction of Methanol with Zinc-Oxide - Single-Crystal Faces and Zinc-Oxide Copper Catalyst Surfaces Studied by Photoelectron-Spectroscopy (XPS and UPS). *Surf. Sci.* **1989**, *221*, 113–130.
74. Nagao, M.; Morimoto, T. Adsorption of Alcohols on Zinc Oxide Surfaces. *J. Phys. Chem.* **1980**, *84*, 2054–2058.
75. Sharma, A.; Singh, B. P.; Dhar, S.; Gondorf, A.; Spasova, M. Effect of Surface Groups on the Luminescence Property of ZnO Nanoparticles Synthesized by Sol-Gel Route. *Surf. Sci.* **2012**, *606*, L13–L17.
76. Kotsis, K.; Staemmler, V. *Ab Initio* Calculations of the O1s XPS Spectra of ZnO and Zn Oxo Compounds. *Phys. Chem. Chem. Phys.* **2006**, *8*, 1490–1498.
77. Takagahara, T. Effects of Dielectric Confinement and Electron-Hole Exchange Interaction on Excitonic States in Semiconductor Quantum Dots. *Phys. Rev. B: Condens. Matter Mater. Phys.* **1993**, *47*, 4569–4585.

78. Xiong, H. M.; Xu, Y.; Ren, O. G.; Xia, Y. Y. Stable Aqueous ZnO@Polymer Core-Shell Nanoparticles with Tunable Photoluminescence and Their Application in Cell Imaging. *J. Am. Chem. Soc.* **2008**, *130*, 7522–7523.
79. Hess, B.; Kutzner, C.; van der Spoel, D.; Lindahl, E. Gromacs 4: Algorithms for Highly Efficient, Load-Balanced, and Scalable Molecular Simulation. *J. Chem. Theory Comput.* **2008**, *4*, 435–447.
80. Groot, R. D.; Warren, P. B. Dissipative Particle Dynamics: Bridging the Gap between Atomistic and Mesoscopic Simulation. *J. Chem. Phys.* **1997**, *107*, 4423–4435.
81. Zhu, Y.-L.; Liu, H.; Li, Z.-W.; Qian, H.-J.; Milano, G.; Lu, Z.-Y. Galamost: GPU-Accelerated Large-Scale Molecular Simulation Toolkit. *J. Comput. Chem.* **2013**, *34*, 2197–2211.
82. Trung Dac, N.; Phillips, C. L.; Anderson, J. A.; Glotzer, S. C. Rigid Body Constraints Realized in Massively-Parallel Molecular Dynamics on Graphics Processing Units. *Comput. Phys. Commun.* **2011**, *182*, 2307–2313.
83. Musa, I.; Massuyeau, F.; Cario, L.; Duvail, J. L.; Jobic, S.; Deniard, P.; Faulques, E. Temperature and Size Dependence of Time-Resolved Exciton Recombination in ZnO Quantum Dots. *Appl. Phys. Lett.* **2011**, *99*, 243107.
84. Zhang, L. Y.; Yin, L. W.; Wang, C. X.; Lun, N.; Qi, Y. X.; Xiang, D. Origin of Visible Photoluminescence of ZnO Quantum Dots: Defect-Dependent and Size-Dependent. *J. Phys. Chem. C* **2010**, *114*, 9651–9658.
85. Tang, Z. Y.; Ozturk, B.; Wang, Y.; Kotov, N. A. Simple Preparation Strategy and One-Dimensional Energy Transfer in CdTe Nanoparticle Chains. *J. Phys. Chem. B* **2004**, *108*, 6927–6931.
86. Solis, D.; Paul, A.; Olson, J.; Slaughter, L. S.; Swanglap, P.; Chang, W. S.; Link, S. Turning the Corner: Efficient Energy Transfer in Bent Plasmonic Nanoparticle Chain Waveguides. *Nano Lett.* **2013**, *13*, 4779–4784.
87. Ghenuche, P.; de Torres, J.; Moparthi, S. B.; Grigoriev, V.; Wenger, J. Nanophotonic Enhancement of the Forster Resonance Energy-Transfer Rate with Single Nanoapertures. *Nano Lett.* **2014**, *14*, 4707–4714.
88. LeBard, D. N.; Levine, B. G.; Mertmann, P.; Barr, S. A.; Jusufi, A.; Sanders, S.; Klein, M. L.; Panagiotopoulos, A. Z. Self-Assembly of Coarse-Grained Ionic Surfactants Accelerated by Graphics Processing Units. *Soft Matter* **2012**, *8*, 2385–2397.